Solution of the Inverse Jet in a Crossflow Problem by a Predictor-Corrector Technique

Joseph R VanderVeer, Yogesh Jaluria*

Department of Mechanical and Aerospace Engineering: Rutgers University, 98 Brett Rd, Piscataway NJ, 08854

Abstract

A predictor-corrector method was modified to suit the inverse jet in a crossflow problem. The methodology was tested against both numerical and experimental data. The jet was generated by heating compressed air with a velocity range of $0 - 5\,m/s$ and temperatures upto $425\,K$. The method attempts to predict the jet velocity, temperature, axial location, and elevation with a self imposed limitation on the quantity of sample points within the domain. The case where all four of the parameters are unknown was determined to be impossible with 9 sample points. The thermal self-similarity of the problem results in an infinite number of solutions to the problem, with no possibility of narrowing the solution count without more information. Knowing the elevation of the jet results in a maximum error of 9%, but typically much better. Experimental tests indicate the methodology is sensitive to error in the sampling data with a few cases reaching and error over 20%. This technique may be extended to applied areas such as exhaust stacks and fuel injection systems.

Keywords: Inverse Problems, Computational Heat Transfer, Convection

1. Introduction

Thermal-fluid systems often create situations in which engineering problem is an inverse heat transfer problem. These problems often have limited

*Corresponding Author

Email address: jaluria@soemail.rutgers.edu (Yogesh Jaluria)

physical access, very limited to no boundary condition knowledge, and/or limited domain knowledge.

For example, the temperature distribution of an optical fiber drawing furnace is difficult to measure directly due to shape, inaccessibility, and high temperatures. The center of the furnace is easily accessible, which directly leads to an inverse heat transfer problem. Issa et al. [1] developed a regularization technique utilizing the centerline temperature, from which the wall temperature may be obtained.

The inverse convection problems have been gaining popularity as late. Prud'homme and Nguyen [2] solved transient inverse convection problems with a single sensor, but the sensor needed to be moved closer to boundary layer as the Rayleigh number increased. Liu et al. [3] determined the thermal profiles in a slot vented enclosure utilizing an iterative approach requiring tens of iterations to achieve less than 1% error.

Another example is the inverse plume in a crossflow problem. The problem entails solving for the plume boundary conditions, utilizing limited domain knowledge. A novel predictor-corrector method was developed by VanderVeer and Jaluria [4] to solve such a problem. The method requires a specific pattern of known points to match exactly against a set of simulations to predict the inverse solution. The specific pattern was optimized to require the least number of known points for plume in a crossflow problem [5]. With zero error in the data a minimum of three known points was possible, however, small amounts of error would require the known point count to increase to at least five.

The present work is the logical progression of the inverse plume in a crossflow problem, the inverse jet in a crossflow problem. The inverse jet in a crossflow problem has many more practical applications, such as exhaust stacks and fuel injection systems. The previous technique will be modified to meet the needs of the new problem.

2. Experimental System

The experiment consists of a wind tunnel with a surface level jet located within the test section. The jet uses compressed air flowing through straighteners to achieve a velocity of U_S and is heated to temperature T_S. The jet is subjected to a perpendicular crossflow of velocity U_∞. Figure 1 is a diagram of the wind tunnel and jet, dimensions are in millimeters.

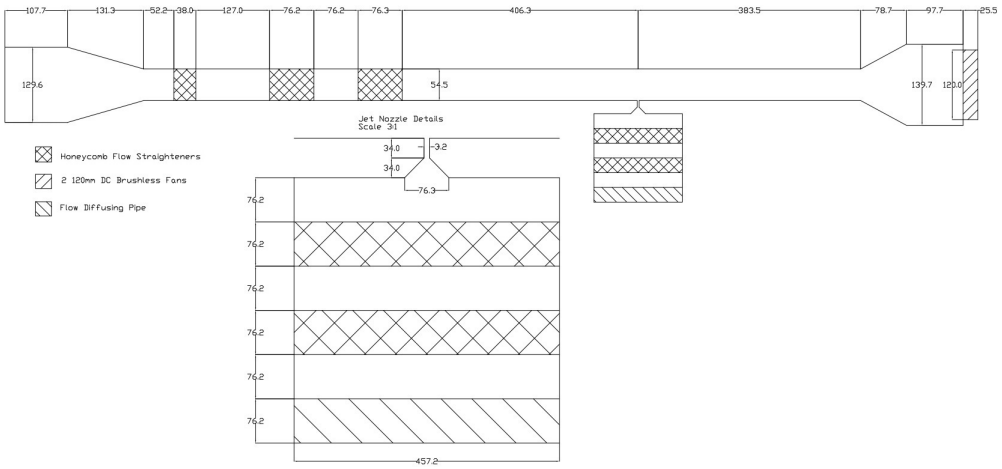

Figure 1: Schematics of the wind tunnel and jet

The wind tunnel test section dimensions are $54.5 \times 305 \times 254\,mm$. The maximum velocity of the wind tunnel is $5.0\,m/s$. The jet is heated by electric cartridge heaters (Omega AHP-7561) with a maximum temperature of $425\,K$, due to material limitations of the wind tunnel. The X-direction is directed downstream of the wind tunnel with the zero at the center of the jet. The Y-direction is in the direction of the jet and is zero at the surface of the wind tunnel. Due to the large aspect ratio of the wind tunnel, the flow is assumed to be two-dimensional.

The free stream velocity is determined by a Pitot-Static tube attached to a NIST traceable differential pressure sensor from Omega(PX655-0.1DI). The pressure sensor has a full scale reading of 0.1 inches of water and is accurate to 0.05% of full scale. This results in a maximum of 3% error of the calculated velocity.

The jet velocity is determined utilizing a rotameter and verified using a Pitot-Static tube attached to the same previously described pressure sensor. This results in the same amount of error of 3% for the jet velocity.

The temperature of domain is measured using a K-type thermocouple mounted to an X-Y traversing stage. Sampled data over the course of several days indicate repeatability of the experiment to within 2%.

3. Numerical Simulations

The simulations were all performed using Ansys Fluent[6]. The Navier-Stokes equations were solved using a three-dimensional, steady state, realizable $k-\epsilon$ model with enhanced wall effects. Conjugate heat transfer is modeled. The free stream Reynolds number is of order 6×10^3, while the jet Reynolds number is between 10^3 and 10^4. The Rayleigh number is of order 10^7.

The governing equations are expressed below:

$$u_i = \overline{u_i} + u_i^{'} \tag{1}$$

$$\frac{\partial \rho}{\partial t} + \frac{\partial}{\partial x_i}\left(\rho u_i\right) = 0 \tag{2}$$

$$\begin{aligned} &\frac{\partial}{\partial t}\left(\rho u_i\right) + \frac{\partial}{\partial x_j}\left(\rho u_i u_j\right) = \\ &\qquad \frac{\partial P}{\partial x_i} + \frac{\partial}{\partial x_j}\left[\mu\left(2S_{ij} - \frac{2}{3}\delta_{ij}\frac{\partial u_k}{\partial x_k}\right) - \rho\overline{u_i^{'}u_j^{'}}\right] \end{aligned} \tag{3}$$

$$\begin{aligned} &\frac{\partial}{\partial t}\left(\rho E\right) + \frac{\partial}{\partial x_i}\left[u_i\left(\rho E + P\right)\right] = \\ &\qquad \frac{\partial}{\partial x_i}\left[\left(\lambda + \frac{C_p \mu_t}{P_{rt}}\right)\frac{\partial T}{\partial x_i}\right] \end{aligned} \tag{4}$$

$$\begin{aligned} &\frac{\partial}{\partial t}\left(\rho k\right) + \frac{\partial}{\partial x_j}\left(\rho k u_j\right) = \\ &\qquad \frac{\partial}{\partial x_j}\left[\left(\mu + \frac{\mu_t}{\sigma_k}\right)\frac{\partial k}{\partial x_j}\right] + \frac{\partial u_j}{\partial x_i}\left(-\rho\overline{u_i^{'}u_j^{'}}\right) \\ &\qquad - g_i \frac{\mu_t}{\rho P_{rt}}\frac{\partial \rho}{\partial x_i} + \rho\epsilon \end{aligned} \tag{5}$$

$$\begin{aligned} &\frac{\partial}{\partial t}\left(\rho\epsilon\right) + \frac{\partial}{\partial x_j}\left(\rho\epsilon u_j\right) = \\ &\qquad \frac{\partial}{\partial x_j}\left[\left(\mu + \frac{\mu_t}{\sigma_\epsilon}\right)\frac{\partial \epsilon}{\partial x_j}\right] + \rho C_1 S\epsilon - \rho C_2 \frac{\epsilon^2}{k + \sqrt{\nu\epsilon}} \\ &\qquad - C_{1\epsilon}\frac{\epsilon}{k}C_{3\epsilon} g_i \frac{\mu_t}{\rho P_{rt}}\frac{\partial \rho}{\partial x_i} \end{aligned} \tag{6}$$

$$-\rho\overline{u_i^{'}u_j^{'}} = 2\mu_t S_{ij} - \frac{2}{3}\delta_{ij}\left(\rho k + \mu_t \frac{\partial u_k}{\partial x_k}\right) \tag{7}$$

The constants for the turbulence model are [7, 8] :

$$C_{1\epsilon} = 1.44, C_2 = 1.9, \sigma_k = 1.0, \sigma_\epsilon = 1.2, P_{rt} = 0.85 \tag{8}$$

$$C_1 = max\left[0.43, \frac{Sk/\epsilon}{Sk/\epsilon + 5}\right], S = \sqrt{2S_{ij}S_{ji}}, C_{3\epsilon} = tanh\left(\frac{u_g}{u_p}\right) \tag{9}$$

$$\mu_t = \frac{\rho C_\mu k^2}{\epsilon} \tag{10a}$$

$$C_\mu = \frac{1}{A_0 + \frac{A_1 k U^*}{\epsilon}} \tag{10b}$$

$$U^* \equiv \sqrt{S_{ij}S_{ji} + \Omega_{ij}\Omega_{ji}} \tag{10c}$$

$$A_0 = 4.04 \tag{10d}$$

$$A_1 = \sqrt{6} cos\left[\frac{1}{3} cos^{-1}\left(\sqrt{6}\frac{S_{ij}S_{jk}S_{ki}}{(S_{ij}S_{ji})^{\frac{3}{2}}}\right)\right] \tag{10e}$$

$$S_{ij} = \frac{1}{2}\left(\frac{\partial u_i}{\partial x_j} + \frac{\partial u_j}{\partial x_i}\right) \tag{10f}$$

$$\Omega_{ij} = \frac{1}{2}\left(\frac{\partial u_i}{\partial x_j} - \frac{\partial u_j}{\partial x_i}\right) \tag{10g}$$

Where the u_g and u_p are the velocity component parallel and perpendicular to gravity respectively.

The inflow boundary conditions are:

$$u = U_\infty, v = 0, T = T_\infty, P = P_\infty, l = 4mm, I = 5\% \tag{11a}$$

$$k = \frac{3}{2}\left(U_\infty I\right)^2 \tag{11b}$$

$$\epsilon = C_\mu^{3/4}\frac{k^{3/2}}{l} \tag{11c}$$

The jet inflow boundary conditions are:

$$u = 0, v = U_S, T = T_S, P = P_\infty, l = 4mm, I = 5\% \tag{12a}$$

$$k = \frac{3}{2}\left(U_\infty I\right)^2 \tag{12b}$$

$$\epsilon = C_\mu^{3/4}\frac{k^{3/2}}{l} \tag{12c}$$

The upper boundary was taken to be symmetric to reduce the possibility of errors by the experimentally accurate no-slip condition. The upper boundary is very far from the jet and therefore should have negligible effect on the numerical result. The bottom of the wind tunnel is made up of $12\,mm$ thick acrylic, while the test section is $25.4\,mm$ thick acrylic. The external boundary conditions are iso-thermal with a temperature of T_∞. The test section external temperature is iso-thermal of $\frac{1}{2}\left(T_S + T_\infty\right)$. The outflow boundary is a simple pressure outflow of P_∞.

3.1. Simulation Validation

A simulation validation study was performed to verify the results of the simulations. Typical verification was performed including flow model, grid independence, and comparison with experimental results. The conditions of the simulation validation are shown in table 1.

The results from Spalart-Allmaras, $k-\epsilon$, and $k-\omega$ were compared and the three models have a similar trend. SA tends to be a bit off, but this is expected due to issues SA has with this type of problem[8]. All of the values were normalized utilizing equation (13), where D is the width of the jet. Figure 2 shows a comparison of the flow models at $X = 4.75$.

$$\phi = \frac{T - T_\infty}{T_S - T_\infty} \tag{13a}$$

$$X = \frac{x}{D} \tag{13b}$$

$$Y = \frac{y}{D} \tag{13c}$$

$$V = \frac{U}{U_\infty} \tag{13d}$$

$$V_S = \frac{U_S}{U_\infty} \tag{13e}$$

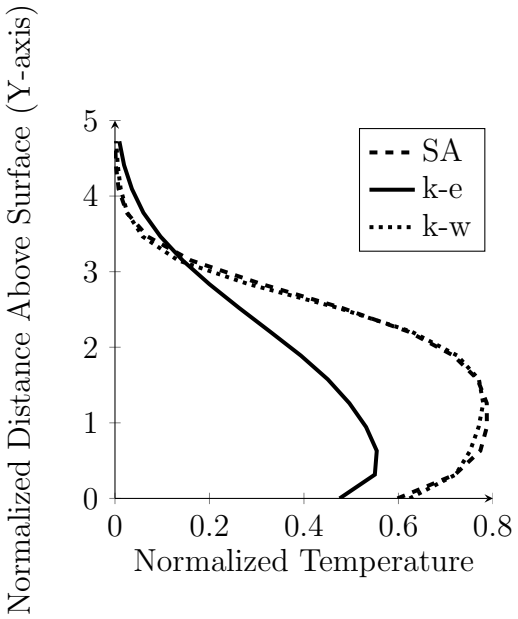

Figure 2: Validation of the simulation: local temperature using three flow models at $X = 4.75$

Grid independence is demonstrated by testing the temperature at a few locations with various grid sizes and geometries, as shown in table 2. Very little variation in simulated temperature over such a wide variety of cell counts shows that the result is most likely grid independent. The grid employed is an unstructured hexagonal mesh with refinement located near the jet and down stream of the jet.

The final validation is comparing the simulation against the experiment. This is done in figure 3. The simulation matches the experiment closely, with the exception of very close to the wall. This is to be expected as the flow models used, even with enhanced wall effects, have difficulty perfectly modeling the near wall conditions.

4. Inverse Solution Methodology

The basis for the solution strategy was described in a paper by VanderVeer and Jaluria [4], which was originally intended to solve the inverse plume in a crosswind. This methodology solved for the 2-D location and source strength of a plume in a crossflow. The jet in a crossflow solver must handle

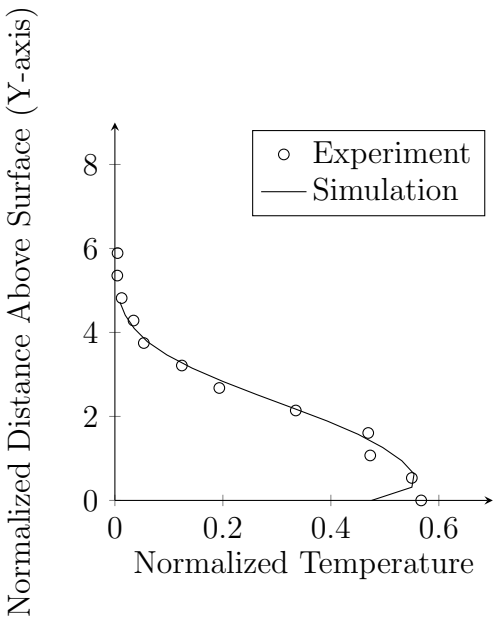

Figure 3: Validation of the simulation: local temperature - experiment versus simulation at $X = 4.75$

one additional parameter, the jet velocity. Therefore the methodology is required to be modified. For completions sake, the original methodology will be briefly described here.

The method assumed that we can neglect the variations in density, thermal buoyancy, and thermal radiation. If this is true, then the temperature of a given location ($T(\boldsymbol{r})$) is linearly dependent upon the source temperature (T_S) as shown in equation (14). The two parameters m and b are both location ($\boldsymbol{r}$) dependent and may be calculated knowing a unique set of simulations A and B.

$$T_S = m(\boldsymbol{r})\, T(\boldsymbol{r}) + b(\boldsymbol{r}) \tag{14a}$$

$$\boldsymbol{r} = r(x, y) \tag{14b}$$

$$\boldsymbol{r}_i = \boldsymbol{r}_0 + \boldsymbol{\Delta}_i \tag{14c}$$

$$m(\boldsymbol{r}) = \frac{T_{SA} - T_{SB}}{T_A(\boldsymbol{r}) - T_B(\boldsymbol{r})} \tag{14d}$$

$$b(\boldsymbol{r}) = T_{SA} - m(\boldsymbol{r})\, T_A(\boldsymbol{r}) \tag{14e}$$

There are a few quick terms to make the following explanation easier.

Sample point: local static temperature from within the domain at a particular location. Datum point: a selected sample point whose location will be defined as $\Delta_0 = (0\,mm, 0\,mm)$. Search shape: relative location and pattern between a set of sample points and a datum point.

Start by selecting n sample points and d simulations. The method attempts to minimize the discrepancies between all of the sample points' calculated source temperature and the datum point's calculated source temperature to get a predicted source temperature. After, minimize the discrepancy between the predicted source temperature and a new set of sample point calculated source temperatures to get the corrected location and temperature. The following equations mathematically describe the previous text. Equation (15) is a minimized at $\boldsymbol{r}^*_{SP}$ and the location $\boldsymbol{r}^*_{SP}$ is used to calculate the predicted source temperature in equation (16). Then equation (17) is minimized at $\boldsymbol{r}_{SP}$ and the location $\boldsymbol{r}_{SP}$ is calculated with equation (18) used to calculate T_{SP}, where a is the number of sample points used in the prediction step and n is the total number of sample points.

$$F(\boldsymbol{r}) = \sum_{i=1}^{a} [m(\boldsymbol{r} + \boldsymbol{\Delta}_i)\, T(\boldsymbol{r}_i) + b(\boldsymbol{r} + \boldsymbol{\Delta}_i) - m(\boldsymbol{r})\, T(\boldsymbol{r}_0) - b(\boldsymbol{r})]^2 \quad (15)$$

$$T^*_{SP} = \frac{1}{a}\{\sum_{i=0}^{a} [m(\boldsymbol{r}^*_{SP} + \boldsymbol{\Delta}_i)\, T(\boldsymbol{r}_i) + b(\boldsymbol{r}^*_{SP} + \boldsymbol{\Delta}_i)]\} \quad (16)$$

$$F_{mod}(\boldsymbol{r}) = \sum_{i=a}^{n} [m(\boldsymbol{r} + \boldsymbol{\Delta}_i)\, T(\boldsymbol{r}_i) + b(\boldsymbol{r} + \boldsymbol{\Delta}_i) - T^*_{SP}]^2 \quad (17)$$

$$T_{SP} = \frac{1}{n-a}\{\sum_{i=a}^{n-a} [m(\boldsymbol{r}_{SP} + \boldsymbol{\Delta}_i)\, T(\boldsymbol{r}_i) + b(\boldsymbol{r}_{SP} + \boldsymbol{\Delta}_i)]\} \quad (18)$$

The number and pattern of the sample points (i.e. the search shape) was optimized in a paper by VanderVeer and Jaluria [5]. In it three sample points were identified as being enough to solve the inverse plume problem. The three points were later shown to not handle error very well and the optimization process was continued to include nine sample points. They are shown in table 3.

Going back to the inverse jet in a crossflow problem, Knight et al. [9] used a quadratic response surface model to determine the jet temperature and jet velocity. Unfortunately, the response surface model used is two dimensional

and would have difficulty applying directly to the current model. The response surface models effectiveness does demonstrate the quadratic nature of the jet velocity and linear nature of jet temperature with respect to local temperature.

The method starts similar to the original method, by selecting n sample points and d simulations spanning the thermal and velocity region of interest. Guess a jet velocity (U_S) so the linear parameters are not dependent upon the jet velocity during the minimization. Calculate the parameters m and b from equation (14). Find the minimization of equation (15) in which we can find a predicted temperature from equation (16). We can develop an equation similar to equation (15) for the jet velocity. Starting with equation (19), we can minimize the discrepancy between the predicted jet velocities resulting in equation (20). As would be expected there are three parameters needed ($\Gamma_0, \Gamma_1, \Gamma_2$). The minimization of G allows U_{SP} to be calculated from equation (21). This new U_{SP} is then used to calculated a new set of linear parameters m and b. The process repeats itself until both the change in U_{SP} and the change in T_{SP} is smaller than some small residual. That is to say $U_{SP} < \epsilon_U$ and $T_{SP} < \epsilon_T$, where ϵ_U and ϵ_T are small values such as $0.01\,m/s$ and $0.1\,K$ respectively. A flowchart of the methodology is shown in figure 4.

$$U_S = \Gamma_2(\boldsymbol{r})\,T(\boldsymbol{r})^2 + \Gamma_1(\boldsymbol{r})\,T(\boldsymbol{r}) + \Gamma_0(\boldsymbol{r}) \tag{19}$$

$$\begin{aligned} G(\boldsymbol{r}) = \sum_{i=a}^{n} [&\Gamma_2(\boldsymbol{r}+\boldsymbol{\Delta}_i)\,T(\boldsymbol{r}_i)^2 \\ &+ \Gamma_1(\boldsymbol{r}+\boldsymbol{\Delta}_i)\,T(\boldsymbol{r}_i) \\ &+ \Gamma_0(\boldsymbol{r}+\boldsymbol{\Delta}_i) \\ &- \Gamma_2(\boldsymbol{r})\,T(\boldsymbol{r}_0)^2 \\ &- \Gamma_1(\boldsymbol{r})\,T(\boldsymbol{r}_0) \\ &- \Gamma_0(\boldsymbol{r})]^2 \end{aligned} \tag{20}$$

$$\begin{aligned} U_{SP} = \frac{1}{n-a}\{\sum_{i=a}^{n-a} [&\Gamma_2(\boldsymbol{r}_{SP}+\boldsymbol{\Delta}_i)\,T(\boldsymbol{r}_i)^2 \\ &+ \Gamma_1(\boldsymbol{r}_{SP}+\boldsymbol{\Delta}_i)\,T(\boldsymbol{r}_i) \\ &+ \Gamma_0(\boldsymbol{r}_{SP}+\boldsymbol{\Delta}_i)]\} \end{aligned} \tag{21}$$

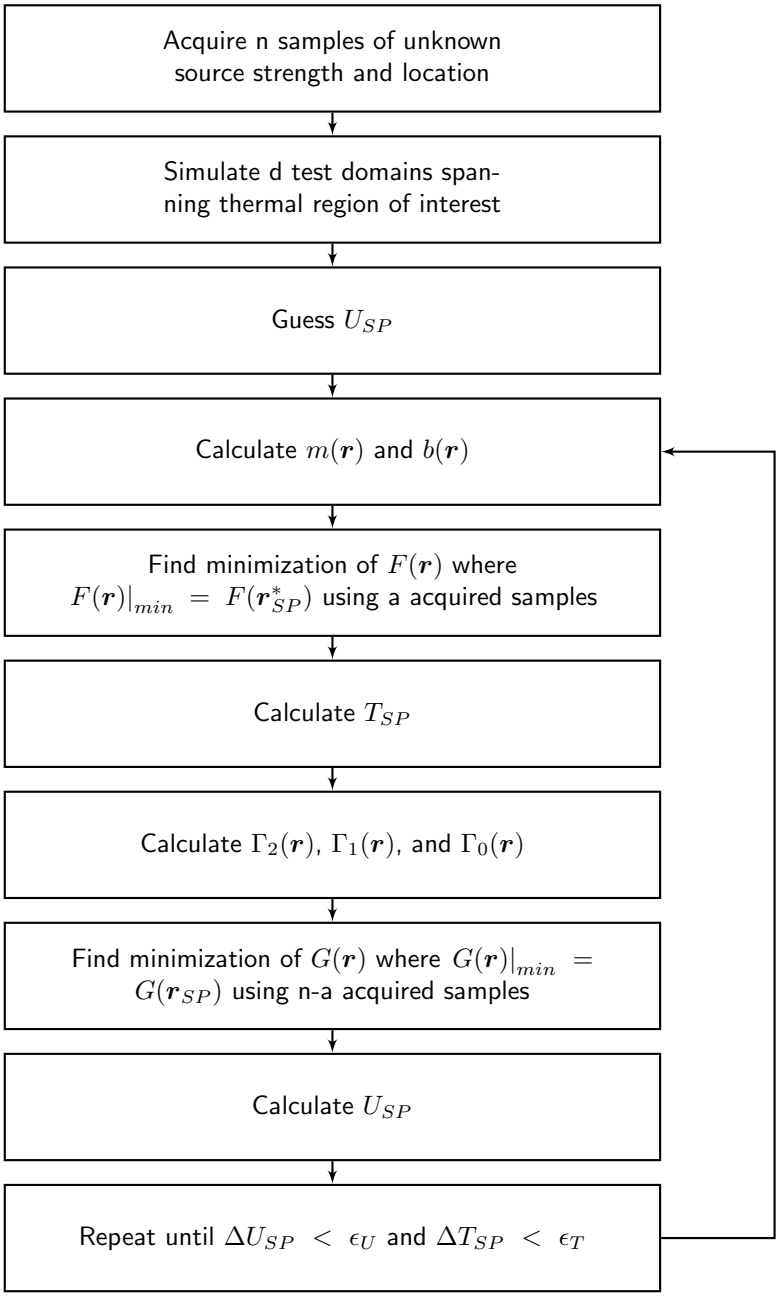

Figure 4: Flow chart of the predictor - corrector methodology for a jet in a crossflow

5. Results and discussions

Due to the new methodology, an incremental approach to solving the problem was used. Work from the simplest steps and moving towards the more difficult cases, ending with the experimental results. The first five steps are of simulated data only, as to separate methodology error from experimental error. Twenty-four selected cases are used to demonstrate the capabilities and weaknesses of the described methodology. The cases are labeled A-X, the conditions of the selected cases are described in table 4 with the constant parameters in table 5. For example, case 'T' has a datum at $20\,mm$ downstream, $3\,mm$ above the surface, jet velocity of $1\,m/s$, and jet temperature of $425\,K$.

The first two steps utilize a single sample point, however, the rest use the nine sample points listed in table 3.

5.1. Source Location and Velocity Known

In the first condition of unknown source temperature, the methodology breaks down to a linear equation, equation (14a). Due to the simple linear equation a single sample point is needed to solve the inverse problem. The results of the selected cases are shown in figure 5. The error is typically less than 0.1%. There are four cases with large error and they are located outside or near the edge of the jet. The temperature at these locations is near the ambient temperature and the Matlab polynomial curve fit has issues with the data points very similar to each other. The error is calculated using equation (22).

$$error_{temp}(\%) = \frac{|T_{SP} - T_S|}{T_S - T_\infty} \times 100 \tag{22a}$$

$$error_{x-location}(\%) = \frac{|x_{SP} - x_S|}{x_S} \times 100 \tag{22b}$$

$$error_{y-location}(\%) = \frac{|y_{SP} - y_S|}{y_S} \times 100 \tag{22c}$$

5.2. Source Location and Temperature Known

The second case is of unknown jet velocity and is also simple and breaks down to equation (19). As the quadratic equation does not perfectly model the velocity profile, the error is still low, as shown in figure 6. The error is less than $\approx 1\%$, which is likely less than that of any experimental error.

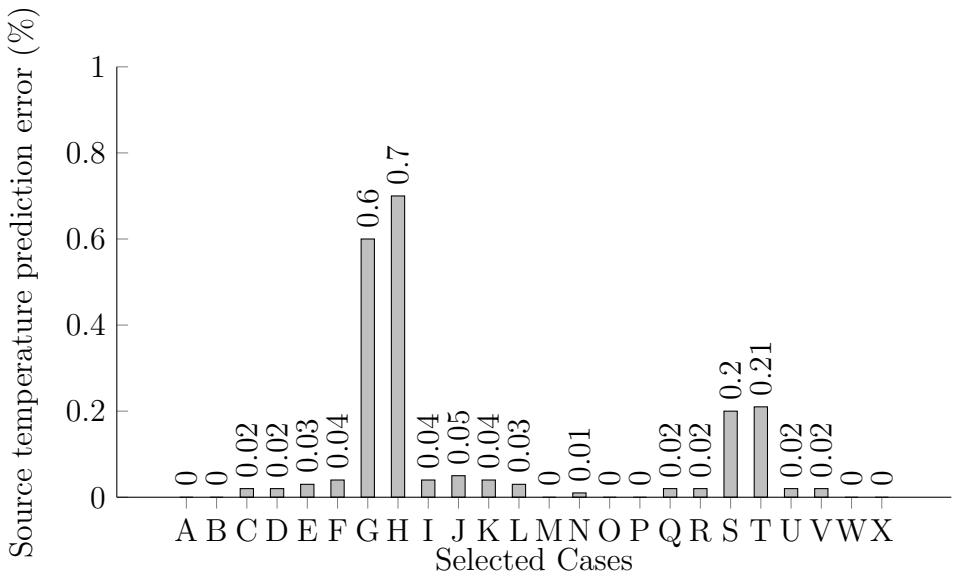

Figure 5: Error in the prediction of T_S from several sampled cases within the jet with $\boldsymbol{r}_S$ and U_S known[10]

5.3. Source Location Known

With only the jet location known, the method would ideally breakdown to the response surface model of Knight et al. [9]. However, the methodology has the jet temperature and jet velocity solved iteratively, and must still be solved in such a manner. The errors of the selected cases are shown in figures 7 and 8. Several of the cases had a decrease in error due to the increase from one sample point to nine.

5.4. Source Elevation Known

Keeping with the incremental stepping, only the source elevation is known. As with the previous step, nine sample points are used. The error results of predicting the source temperature, velocity, and axial location are shown in figures 9 to 11. The max error increases significantly to 9%, but typical values are much less and reasonable for inverse problems.

5.5. Source Location and Strength Unknown

The final incremental step is not possible with the current methodology and search shape. The underlying, self-similar characteristics of a jet in

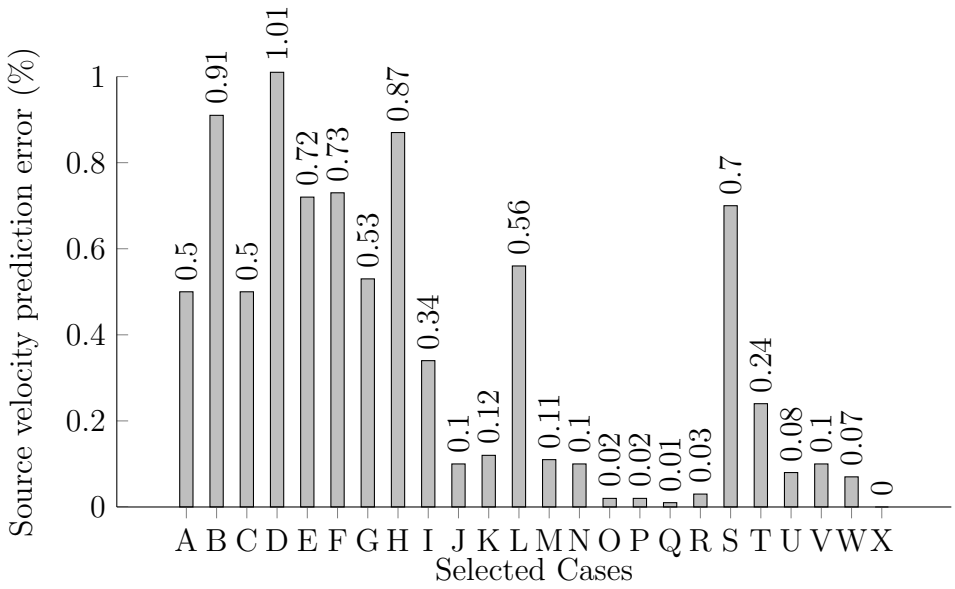

Figure 6: Error in the prediction of U_S from several sampled cases within the jet with $\boldsymbol{r}_S$ and T_S known[10]

a crossflow creates an indiscernible infinite set of possible solutions. It is possible that a significant increased sample size would alleviate the problem, but the goal of this work was to utilize very limited domain information.

As an example, a set of alternate solutions is shown in table 6 for case 'V'. This list was not meant to be comprehensive, but rather illustrative of the problem. The last column is the percent error between the various solutions.

5.6. Experimental Results

Due to the last step we will only consider searching for the source temperature, velocity, and axial location for the experimental cases. The experimental conditions are listed in table 7. A select few results are shown in table 8. A table format was chosen to represent the data, as the error is significant and would make a chart difficult to read.

A graph of actual vs predicted source temperature and velocity are shown in figures 12 and 13 respectively. It is easily visualized that this methodology predicts the source velocity significantly better than source temperature. The large percentages are due to the velocities being small. Often, the predicted error is close to the experimental error of the system.

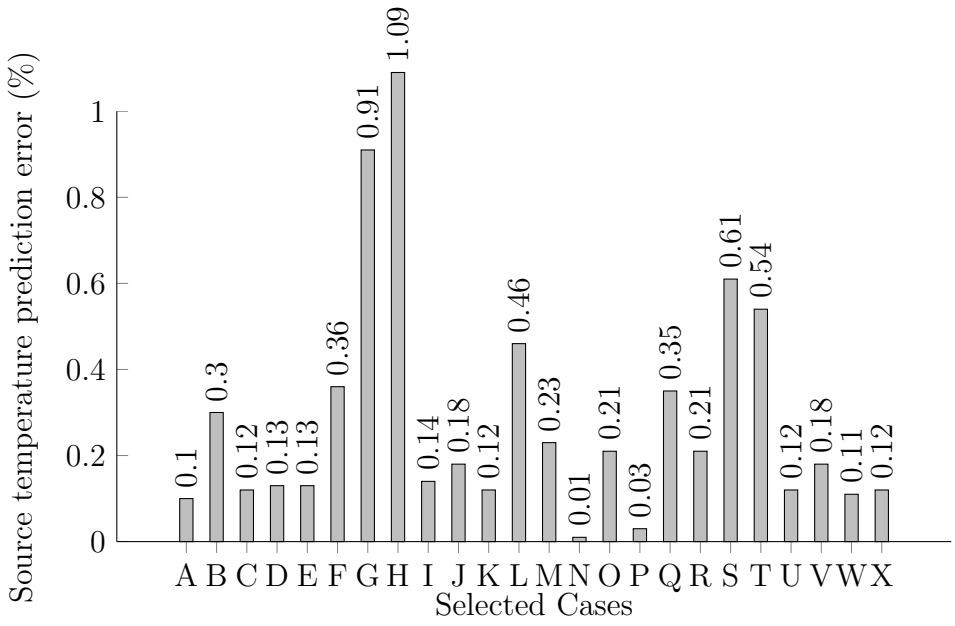

Figure 7: Error in the prediction of T_S from several sampled cases within the jet with $\boldsymbol{r}_S$ known[10]

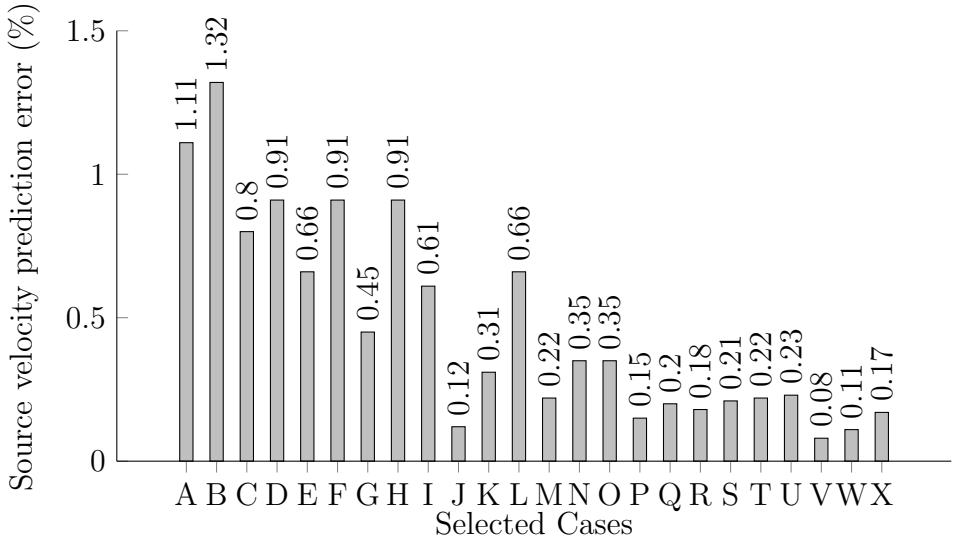

Figure 8: Error in the prediction of U_S from several sampled cases within the jet with $\boldsymbol{r}_S$ known[10]

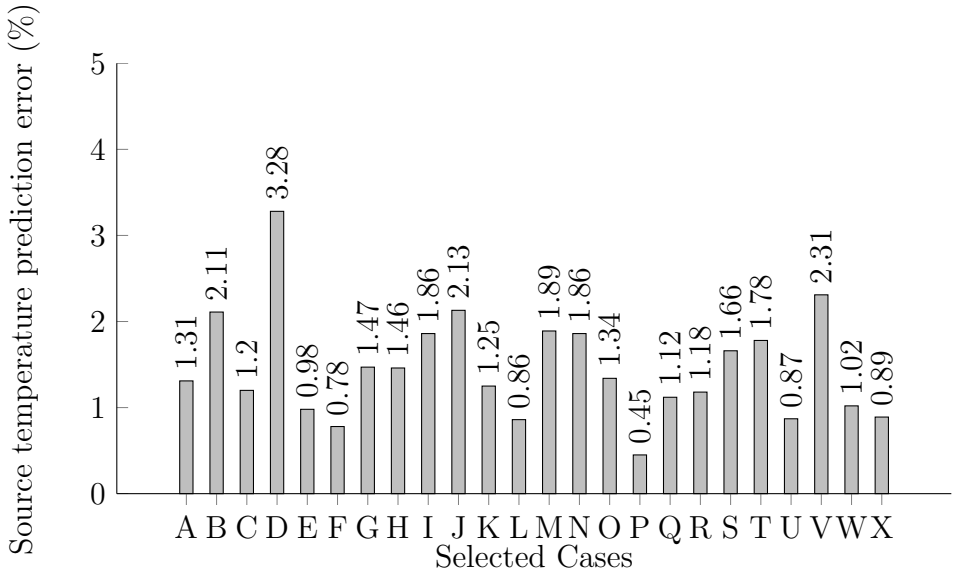

Figure 9: Error in the prediction of T_S from several sampled cases within the jet with source elevation known[10]

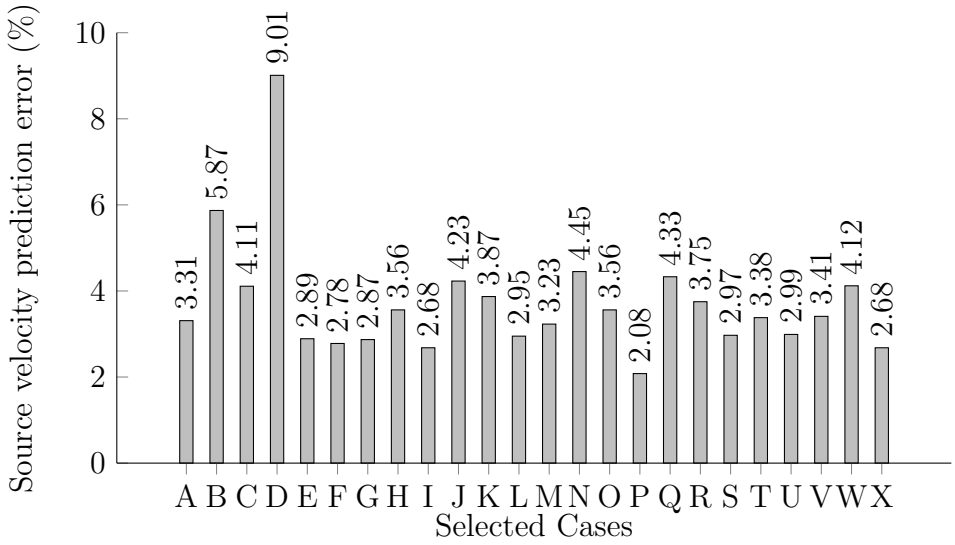

Figure 10: Error in the prediction of U_S from several sampled cases within the jet with source elevation known[10]

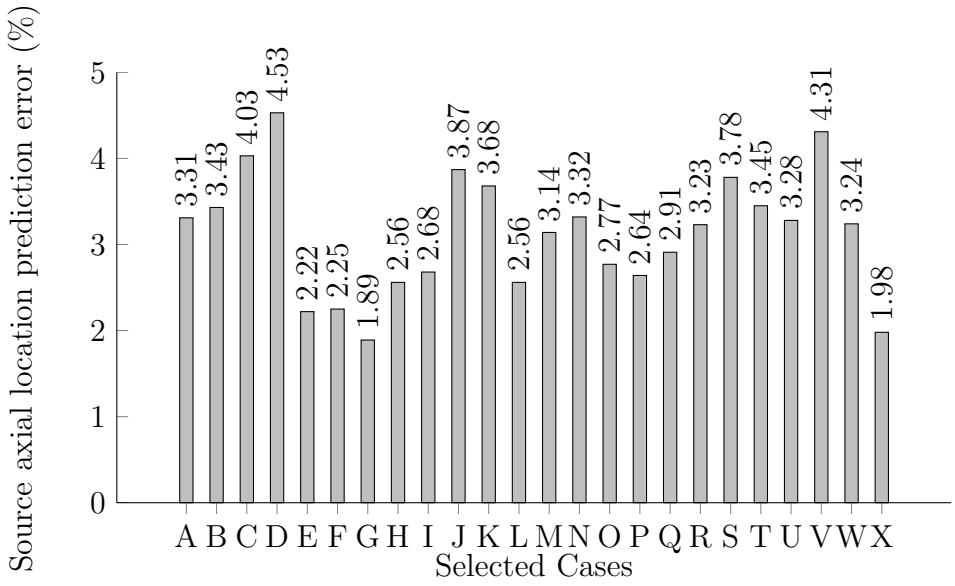

Figure 11: Error in the prediction of x_S from several sampled cases within the jet with source elevation known[10]

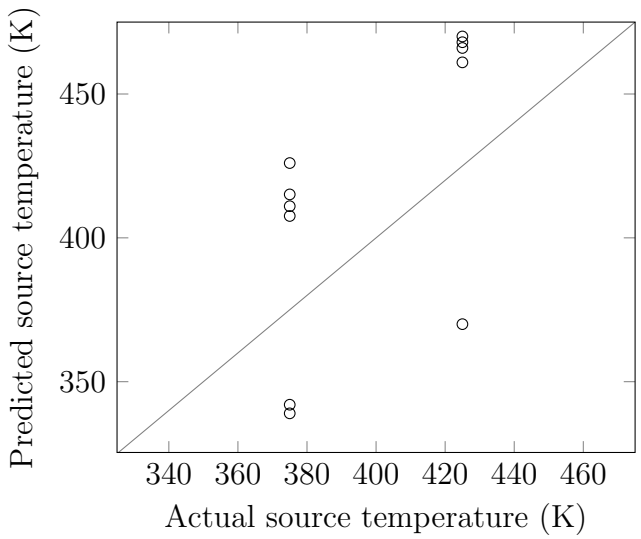

Figure 12: Actual vs predicted source temperature for several cases within the jet

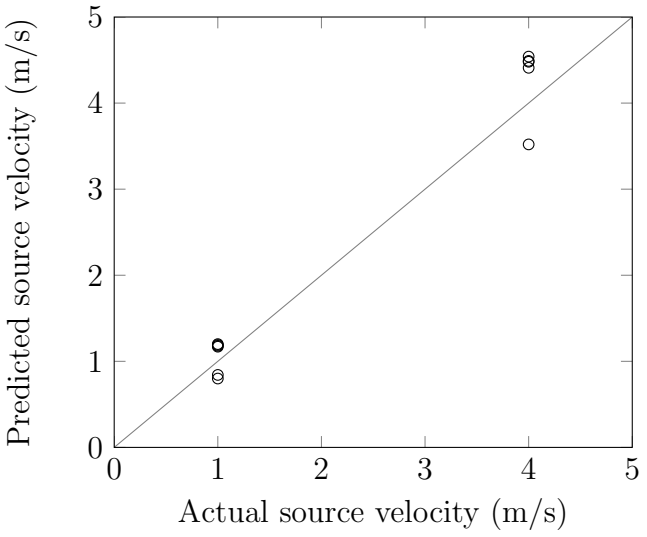

Figure 13: Actual vs predicted source velocity for several cases within the jet

6. Conclusions

A predictor-corrector method was modified and applied to the inverse jet in a crossflow problem. The inverse method was previously developed and the search shape was optimized. Four parameters were searched for source temperature, velocity, axial location, and elevation. The new methodology functioned accurately for 4 out of 5 steps, with all four parameters unknown being the exception. There was not enough information to accurately discern the solution from the infinite solution set. Other than the exception, the methodology performed well with approximately 9% even in the worst cases, and typically performing much better.

The step utilizing experimental results showed a significantly worse error. This indicates that this methodology, when applied to the jet in a crossflow problem, is somewhat error sensitive. However, the jet velocity prediction error was close to that experimental jet velocity error.

Previous optimization of the search shape indicates that the methodology is sensitive to the search shape[5]. More work on the inverse jet in a crossflow problem, by optimizing the search shape specifically for the jet problem, may reduce the overall error.

The methodology has demonstrated its capabilities and limitations, and much more work may be done regarding the limitations. There are several improvements still needing to be made, such as three dimensional capabilities, transient capabilities, and possibly the ability to differentiate multiple sources. These features, if implemented, would have significant applications to fires in urban environments and pollution in industrial areas.

References

[1] J. Issa, Z. Yin, C. E. Polymeropoulos, Y. Jaluria, Temperature distribution in an optical fiber draw tower furnace, Journal of Materials Processing and Manufacturing Science vol 4 (1996) 221–232.

[2] M. Prud'homme, T. H. Nguyen, Solution of inverse free convection problems by conjugate gradient method: effects of rayleigh number, International Journal of Heat and Mass Transfer vol44 (2001) 2011–2027.

[3] D. Liu, F.-Y. Zhao, H.-Q. Wang, E. Rank, G.-X. Kou, Inverse determination of building heating profiles from the knowledge of measurements

within the turbulent slot-vented enclosure, International Journal of Heat and Mass Transfer vol 55 (2012) 4597–4612.

[4] J. VanderVeer, Y. Jaluria, Solution of an inverse convection problem by a predictor-corrector approach, International Journal of Heat and Mass Transfer vol65 (2013) 123–130.

[5] J. VanderVeer, Y. Jaluria, Optimization of an inverse convection solutions strategy, International Journal of Heat and Mass Transfer 73 (2014) 664–670.

[6] Ansys, Fluent (version 13), 2010.

[7] T. hsing Shih, W. Liou, A. Shabbir, Z. Yang, J. Zhu, A new $k-\epsilon$ eddy viscosity model for high reynolds number turbulent flows, Computer Fluids vol 24 (1995) 227–238.

[8] Ansys, Fluent Technical Documents v14.0, Technical Report, Ansys, 2011.

[9] D. Knight, Q. Ma, T. Rossmann, Y. Jaluria, Evaluation of fluid-thermal systems by dynamic data driven application systems - part ii, in: International Conference on Modeling and Optimization of Structures, Processes and Systems, Springer-Verlag, University of Kwazulu-Natal, South Africa, 2007.

[10] J. VanderVeer, Solutions of Inverse Convection Problems by a Predictor-Corrector Technique, Ph.D. thesis, Rutgers University, 2014.

Nomenclature

$\boldsymbol{r}$	vector location of sampled points
a	number of sample locations used in the predictor stage
$b, m, \Gamma_0, \Gamma_1, \Gamma_2$	model parameters
$C_1, C_2, C_{1\epsilon}, C_\mu, \sigma_k, \sigma_\epsilon$	$k-\epsilon$ model coefficients
d	number of simulations
E	thermal energy
F	minimization function for temperature
G	minimization function for velocity
k, ϵ	turbulence kinetic energy, dissipation rate
l, I	turbulence length scale and intensity
n	number of sample locations
P	pressure
P_{rt}	turbulent Prandtl number
T	temperature
t	time
U	free stream velocity
X, Y	normalized coordinates
x, y	coordinates

Greek Symbols

$\boldsymbol{\Delta}$	relative difference between the first sampled point and other sampled points
$\boldsymbol{\delta}$	vector distance between the actual sampled location and the current test location
λ	thermal conductivity
μ	dynamic viscosity
μ_t	eddy viscosity
ϕ	normalized temperature $\phi = \frac{T-T_\infty}{T_S-T_\infty}$
ρ	density
ε	error associated with the inverse convection method at a location with given sampled data

Superscripts

$*$	predictor stage, alternative heat flux eqn.

Subscripts

$0, 1, 2$	sample point indexes
∞	free stream
A, B	data set A,B
i, j, k	index
mod	modified
O	optimized
P	predicted
S	source

Parameter	Value
$U_\infty\,(m/s)$	2.0 ± 0.02
$U_S\,(m/s)$	2.0 ± 0.2
$T_\infty\,(K)$	305 ± 0.5
$P_\infty\,(kPa)$	101.3 ± 0.01
$T_S\,(K)$	350 ± 2.0

Table 1: Validation test conditions

Location (x,y) (mm)	0,1	10,5	15,5	30,10
Cell Count				
57660	337.7	323.3	321.6	310.1
83888	337.7	323.3	321.6	310.1
166352	337.7	323.2	321.5	310.1
366168	337.7	323.2	321.5	310.1

Table 2: Grid Independence Study, local static temperature (K)

Sample Point	$\mathbf{\Delta}\,(mm)$
0	(0.0, 0.0)
1	(1.7, 3.5)
2	(2.8, 0.6)
3	(0.5, 1.1)
4	(2.1, 1.0)
5	(2.3, 2.0)
6	(1.2, 0.8)
7	(3.1, 0.7)
8	(0.8, 2.1)

Table 3: Search shape results of averaging over the domain with increasing the sample size to 9

U_S (m/s)	1	1	2	2	4	4
T_S (K)	375	425	375	425	375	425
Location (x,y) 10 mm, 1 mm	A	B	C	D	E	F
10 mm, 3 mm	G	H	I	J	K	L
20 mm, 1 mm	M	N	O	P	Q	R
20 mm, 3 mm	S	T	U	V	W	X

Table 4: Several sampled case parameters

Parameter	Value
$U_\infty\,(m/s)$	2
$T_\infty\,(K)$	293
$P_\infty\,(kPa)$	101.3

Table 5: Simulation test conditions

Axial Loc. (mm)	Elev. Loc. (mm)	Jet Temp. (K)	Jet Vel. (m/s)	Search Shape Error (%)
20.0	3.0	425	2.0	0.00
10.0	3.7	375	2.5	0.60
12.0	5.1	375	3.0	0.34
14.8	2.7	400	2.0	0.30
16.3	4.5	400	2.5	0.26
19.5	5.9	400	3.0	0.29
21.8	5.0	425	2.5	0.24
25.6	6.5	425	3.0	0.34
25.2	3.2	450	2.0	0.13
26.8	5.4	450	2.5	0.25

Table 6: Example alternative solutions[10]

Parameter	Value
$T_\infty\,(K)$	297.6 ± 8.0
$P_\infty\,(kPa)$	100.6 ± 0.6
$U_\infty\,(m/s)$	2.0 ± 0.02

Table 7: Experimental test conditions

$U_S\ (m/s)$		1.0	1.0	4.0	4.0
$T_S\ (K)$		375	425	375	425
Location (x,y)					
10 mm, 0 mm	X	10.9%	11.7%	11.1%	13.8%
	U	21.8%	18.6%	10.4%	11.9%
	T	8.70%	9.87%	10.7%	12.9%
20 mm, 0 mm	X	8.65%	7.65%	5.40%	9.81%
	U	18.7%	19.8%	11.5%	12.1%
	T	8.81%	10.7%	9.65%	10.2%
30 mm, 0 mm	X	10.6%	10.4%	18.7%	9.78%
	U	15.8%	17.9%	12.3%	13.7%
	T	9.61%	8.64%	13.7%	10.1%

Table 8: Error in predicting source axial location (x_S), source strength(U_S and T_S) from a few sample cases within the jet, search shape with 9pts, utilizing experimental data[10]